Modeling bulk and surface Pt using the "Gaussian and plane wave" density functional theory formalism: Validation and comparison to k-point plane wave calculations

Santarossa, Gianluca ; Vargas, Angelo ; Iannuzzi, Marcella ; Pignedoli, Carlo A ; Passerone, Daniele ; Baiker, Alfons

Abstract: We present a study on structural and electronic properties of bulk platinum and the two surfaces (111) and (100) comparing the Gaussian and plane wave method to standard plane wave schemes, normally employed for density functional theory calculations on metallic systems. The aim of this investigation is the assessment of methods based on the expansion of the Kohn-Sham orbitals into localized basis sets and on the supercell approach, in the description of the metallicity of Pt. Electronic structure calculations performed at Gamma-point only on supercells of different sizes, from 108 up to 864 atoms, are compared to the results obtained for the unit cell of four Pt atoms where the k-point expansion of the wave function over Monkhorst-Pack grids up to (10x10x10) has been employed. The evaluation of the two approaches with respect to bulk properties is done through the calculation of the equilibrium lattice constant, the bulk modulus, and the total and the d-projected density of states. For the Pt(111) and Pt(100) surfaces, we consider the relaxation of the first layers, the surface energies, the work function, the total density of states, as well as the center and filling of the d bands. Our results confirm that the accuracy of two approaches in the description of electronic and structural properties of Pt is equivalent, providing that consistent supercells and k-point meshes are used. Moreover, we estimate the supercell size that can be safely adopted in the Gaussian and plane wave method in order to obtain the same reliability of previous theoretical studies based on well converged plane wave calculations available in literature. The latter studies, in turn, set the level of agreement with experimental data. In particular, we obtain excellent agreement in the evaluation of the density of states for either bulk and surface systems, and our data are also in good agreement with previous works on Pt reported in literature. We conclude that Gaussian and plane wave calculations, with simulation cells of 400-800 atoms, can be safely used in the study of chemistry related problems involving transition metal surfaces.

DOI: https://doi.org/10.1063/1.3037227

DOI: https://doi.org/10.1063/1.3037227

Modeling bulk and surface Pt using the "Gaussian and plane wave" density functional theory formalism: Validation and comparison to k-point plane wave calculations

Gianluca Santarossa, Angelo Vargas, Marcella Iannuzzi, Carlo A. Pignedoli, Daniele Passerone, and Alfons Baiker'

Citation: The Journal of Chemical Physics **129**, 234703 (2008); doi: 10.1063/1.3037227
View online: http://dx.doi.org/10.1063/1.3037227
View Table of Contents: http://aip.scitation.org/toc/jcp/129/23
Published by the American Institute of Physics

Modeling bulk and surface Pt using the "Gaussian and plane wave" density functional theory formalism: Validation and comparison to *k*-point plane wave calculations

Gianluca Santarossa,[1] Angelo Vargas,[1] Marcella Iannuzzi,[2] Carlo A. Pignedoli,[3] Daniele Passerone,[3] and Alfons Baiker[1,a)]

[1]*Department of Chemistry and Applied Biosciences, Institute for Chemical and Bioengineering, ETH Zurich, Hönggerberg, HCI, CH-8093 Zurich, Switzerland*

[2]*Laboratory for Reactor Physics and System Behavior, Paul Scherrer Institut, CH-5232 Villigen, Switzerland*

[3]*Empa, Swiss Federal Laboratories for Materials Testing and Research, Nanotech@surfaces Laboratory, CH-8600 Dübendorf, Switzerland*

(Received 20 June 2008; accepted 3 November 2008; published online 15 December 2008)

We present a study on structural and electronic properties of bulk platinum and the two surfaces (111) and (100) comparing the Gaussian and plane wave method to standard plane wave schemes, normally employed for density functional theory calculations on metallic systems. The aim of this investigation is the assessment of methods based on the expansion of the Kohn–Sham orbitals into localized basis sets and on the supercell approach, in the description of the metallicity of Pt. Electronic structure calculations performed at Γ-point only on supercells of different sizes, from 108 up to 864 atoms, are compared to the results obtained for the unit cell of four Pt atoms where the *k*-point expansion of the wave function over Monkhorst–Pack grids up to $(10\times10\times10)$ has been employed. The evaluation of the two approaches with respect to bulk properties is done through the calculation of the equilibrium lattice constant, the bulk modulus, and the total and the *d*-projected density of states. For the Pt(111) and Pt(100) surfaces, we consider the relaxation of the first layers, the surface energies, the work function, the total density of states, as well as the center and filling of the *d* bands. Our results confirm that the accuracy of two approaches in the description of electronic and structural properties of Pt is equivalent, providing that consistent supercells and *k*-point meshes are used. Moreover, we estimate the supercell size that can be safely adopted in the Gaussian and plane wave method in order to obtain the same reliability of previous theoretical studies based on well converged plane wave calculations available in literature. The latter studies, in turn, set the level of agreement with experimental data. In particular, we obtain excellent agreement in the evaluation of the density of states for either bulk and surface systems, and our data are also in good agreement with previous works on Pt reported in literature. We conclude that Gaussian and plane wave calculations, with simulation cells of 400–800 atoms, can be safely used in the study of chemistry related problems involving transition metal surfaces. © *2008 American Institute of Physics*. [DOI: 10.1063/1.3037227]

I. INTRODUCTION

The determination of the properties of metal surfaces attracts a wide scientific and technological interest, ranging from catalysis to electrochemistry, corrosion, and lubrication.[1–8] Due to their extensive application in catalysis, platinum surfaces, in particular, have been subject of extensive experimental and theoretical investigations. Platinum surface structures have been studied using low-energy electron diffraction spectroscopy[9–13] (LEEDS) and ion scattering microscopy.[14–16] The electronic structure, instead, has been determined by means of angle-resolved photoemission experiments,[17] while ultraviolet photoemission spectroscopy has been used for accurate estimates of the Pt(111) work function.[18] After the pioneering works of Lang and Kohn,[19–23] accurate calculations of Pt bulk and (111) surface[24–34] played an important role in the prediction of the behavior of the solid metal for technical applications. State-of-the-art computational studies of bulk Pt and Pt surfaces[24,25] are based on density functional theory (DFT),[35] within the independent particle formalism of Kohn and Sham,[36] and employ the general gradient approximation (GGA) for the exchange-correlation functionals. We note in passing that some studies seem to indicate that properties such as the work function are better described by pure local density approximation (LDA) in the case of Pt.[37] This fact could be due to a cancellation of errors, and we will not investigate it further within this work.

In standard implementations of DFT for calculations on solid state systems– in particular, with metallic character– the wave functions and the charge density are expanded in plane waves (PWs) and the band structure is accurately

a)Electronic mail: baiker@chem.ethz.ch. Tel.: +41 44 6323153. Fax: +41 44 6321163.

evaluated through proper sampling of the Brillouin zone (BZ). An exhaustive list of the most popular program packages for this type of applications can be found in Ref. 38. Indeed, orthogonal and originless PW basis sets are often considered the natural choice to represent the electronic density of periodic systems. They are typically used in combination with linear scaling algorithms to solve the Poisson equation in reciprocal space, the efficiency of fast Fourier transforms (FFT) can be directly exploited to obtain real space representations, and the implementation of the *k*-point expansion is straightforward. The description through PW and *k*-point expansions is established as the most efficient and accurate scheme for static calculations of bulk properties, when the simple unit cell associated with a properly large Monkhorst–Pack (MP) mesh[39] is sufficient to represent the system, and algorithms exploiting the lattice symmetry can be employed. Similar approaches have been applied also in the study of mechanisms in the field of heterogeneous catalysis.[1–5] However, small simulation cells and static calculations are rather strong limitations in the investigation of catalytic surfaces and chemisorption phenomena. Actually, the desirable features for such simulations are large surface areas, in order to accommodate reactants, products, and possible surface functionalities, as well as the inclusion of finite temperature effects through the generation of molecular dynamics trajectories.[40,41] Moreover, basis sets constituted of localized orbitals are normally preferred for the description and the interpretation of the surface chemistry in terms of molecular orbitals, whereas the use of PW can become rather inefficient for systems containing large empty regions.

In this perspective, we are looking for a DFT implementation which makes use of accurate and compact basis sets and is suited for molecular dynamics simulations of large condensed matter systems at relatively limited computational costs. Approaches based purely on a linear combination of atomic orbitals (LCAO) need a basis set that is as accurate as possible, particularly in the case of metals and, even more, when modeling molecular adsorption on metals. Systematic studies focused on the latter class of problems are available.[42–47] Among the DFT implementations based on localized basis sets, the CRYSTAL (Ref. 48) and SIESTA (Ref. 49) packages have been successfully used for simulations of solid state systems.[26,42–47] The equivalence between computational approaches based on a description of the wave function with PW or localized orbitals has been already discussed by several authors.[42–47] However, a systematic validation of the supercell approach for the calculation of transition metal surface properties is still missing. In this work, we evaluate the accuracy and efficiency of Γ-point only calculations carried out by the Gaussian and plane wave (GPW) method,[50,51] as implemented in the CP2K code, in the case of bulk Pt, Pt(111) surface, and Pt(100) surface. The validation is carried out through the comparison with results obtained by applying the PW and *k*-point formalism, as implemented into two other DFT codes, ABINIT (Ref. 52) and PWSCF (Ref. 53), as well as with computed and experimental data already available in the literature. The GPW method uses atom-centered Gaussian-type orbitals (GTOs) to describe the wave functions and an auxiliary PW basis set for the expansion of the charge density in reciprocal space. In this way, the advantages of the two representations are combined. Thanks to the compact description of the wave function by GTO, efficient algorithms can be used that take advantage of the sparsity of the Kohn–Sham, overlap, and density matrix, which becomes even more pronounced by increasing the system size.[54] On the other hand, the expansion of the charge density in PW allows the FFT based treatment of the Poisson equation, leading to linear scaling calculation of the Hartree energy.[55]

In order to be able to investigate the chemistry of complex molecules at surfaces, two requisites have to be met: (a) large simulation cells, i.e., forming a slab with adequate surface area and number of layers to model molecular adsorption; (b) relatively limited computational costs for both electronic structure and forces, since many configurations need to be considered in the investigation of stationary states and reaction pathways. GPW is known to scale almost linearly with the system size, while standard PW codes typically scale quadratically. For this reason, GPW should be a better choice for calculations on very large systems. Several recent applications, indeed, demonstrate that the method is well suited for simulation of large condensed systems, such as liquids and solids.[56–58] In order to compare roughly the computational efficiency of the GPW method with the standard PW approach when a large unit cell must be used, a test calculation has been performed: A single iteration along a self-consistent field (SCF) wave function optimization, performed at Γ-point only for a simulation cell of 256 Pt atoms, takes ~300 s by using PWSCF with an ultrasoft pseudopotential and energy cutoff of 30 Ry, while ~9 are needed by GPW with a TVZP basis set, a norm-conserving pseudopotential, and 300 Ry as energy cutoff for the density (64 cores on CRAY XT3).

From band structure theory, it is known that the eigenvectors of the electronic problem in a periodic system are labeled by vectors (**k**-vectors) in the reciprocal space, ranging in the so-called first BZ (FBZ). The charge density obtained from a periodic calculation including only the elementary unit cell is correct only if obtained through the integration over the whole FBZ and remains accurate if an adequate finite number of **k**-vectors is selected. In particular, one can choose (although it is not the optimal choice) a regular $(n\times n\times n)$ grid centered at $\mathbf{k}=\mathbf{0}$ (the so-called Γ-point). This choice is equivalent to a calculation done with a $(n\times n\times n)$ supercell where the density is computed at the Γ-point only. This latter approach is mandatory when dealing with surface molecular adsorption [see requisite (a) above] and is the one used for our GPW calculations. The PW calculations presented in this work, instead, are done on small unit cells expanding the wave function over a set of **k**-vectors that guarantees equivalence to the supercell approach at the Γ-point. In addition, some denser grid of **k**-vectors have been also used in order to check the adequacy of the supercell size with respect to electronic properties.

II. COMPUTATIONAL METHODS

A. GPW simulations

We use the latest implementation of the GPW formalism in the Quickstep module of the CP2K program package, a suite of programs aimed at performing efficient electronic structure calculations and molecular dynamics at different levels of theory.[55] The Kohn–Sham orbitals are expanded in terms of contracted GTO,

$$\psi_i(\mathbf{r}) = \sum_\alpha C_{\alpha i}\varphi_\alpha(\mathbf{r}), \tag{1}$$

where ψ_i is the molecular orbital corresponding to the ith Kohn–Sham state, $\{\varphi_\alpha\}$ are the basis set functions, and $\{C_{\alpha i}\}$ the expansion coefficients. The auxiliary PW basis set is, instead, used only to expand the electronic charge density for the calculation of the Hartree potential. In order to limit the number of PW functions, the interaction of the valence electrons with frozen atomic cores is described via the use of norm-conserving, dual-space-type pseudopotentials (PP).[59] In particular, we used a PP that includes the $5s$ and $5p$ semicore electrons in the valence, thus treating 18 electrons explicitly. The GTO basis set has been optimized for the specific Pt-PP. We found that the triple-zeta valence (TZV) basis set, with very confined functions (smallest exponent of 0.1), is the optimal choice in terms of efficiency and accuracy for solid state Pt. For the auxiliary PW expansion of the charge density, the energy cutoff has been set at 300 Ry. The exchange and correlation term was modeled using the Perdew–Burke–Ernzerhof (PBE) functional.[60] For the solution of the SCF equations, we used an optimizer based on orbital transformations, which scales linearly in the number of basis functions.[61] It has been already demonstrated that this optimization algorithm, in combination with the GPW linear scaling calculation of the Kohn–Sham matrix, can be used for applications with several thousands of basis functions.[58] Geometry optimizations have been carried out using the Broyden–Fletcher–Goldfarb–Shanno (BFGS) minimization algorithm,[62–66] and the structures have been optimized until the atomic displacements were lower than 3×10^{-3} Bohr and the forces lower than 4.5×10^{-4} Hartree/Bohr.

To model the bulk within the GPW formalism, we used four supercells of increasing size. These have been generated by replicating the conventional unit cell (four atoms) n times along the three Cartesian axis, where n ranges from 3 to 6. The resulting four models contain 108 (n=3), 256 (n=4), 500 (n=5), and 864 (n=6) Pt atoms, respectively. In order to compare the results obtained with these supercells with the results of the PW calculations at the same level of accuracy, throughout the paper the supercells will be named after the number of replica of the unit cell n, i.e., $(3\times3\times3)$, $(4\times4\times4)$, etc. It is important to note here that the chosen nomenclature does not directly reflect the number of atoms contained in the supercell. For example, the supercell employed for the case n=4 $(4\times4\times4)$, which is shown in Fig. 1(a), contains eight Pt atoms for each side, for a total number of 256 Pt atoms. The equilibrium lattice constant and the bulk modulus have been determined for each of the four cases by varying the side length between $(3.920\times n)$ Å and $(3.980\times n)$ Å and running a new geometry optimization at each volume.

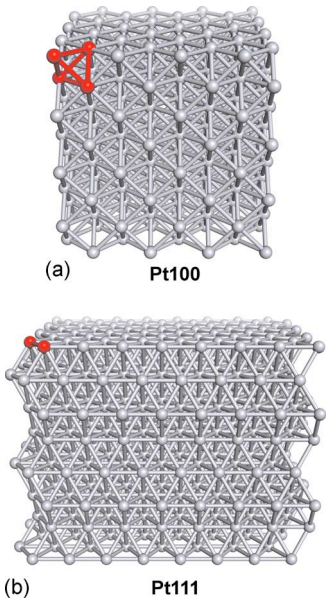

FIG. 1. (Color online) Examples of supercells employed in the GPW calculations. The unit cells are highlighted in a different color (red) at the higher left corner of each supercell. (a) Supercell exposing the (100) crystallographic plane. The supercell has a total number of 256 Pt atoms, distributed among eight layers. This supercell is used for the calculations of both the bulk and the Pt(100) surface. (b) Supercell exposing the (111) crystallographic plane. The supercell is made of eight layers with 64 Pt atoms each.

In order to model the Pt surfaces, we used the standard slab approach, where the semi-infinite bulk is approximated by a finite number of atomic layers, parallel to the desired crystallographic plane. The resulting slab is separated from its periodic images in the direction perpendicular to the surface by interposing an adequate amount of empty space (more than 15 Å in our case). In order to correctly extract surface properties from a calculation done on a slab, its thickness should be sufficiently large to guarantee a bulklike behavior in its interior. In the case of Pt(111), for the sake of simplicity our surface unit cell was set as a rectangular cell made up of two rhombohedral unit cells, resulting in (8×8) atoms per layer, piled along the z axis. In order to estimate the effects of the slab approximation (i.e., finite number of layers), we computed the surface properties for six different samples by increasing the number of layers from 3 to 8. The supercell used for the simulation of the Pt(111) surface with eight layers is shown in Fig. 1(b). The unit cell of two Pt atoms is evidenced in a different color (red) in the higher left corner of the picture. In order to generate the correct atomic pattern, the unit cell is replicated eight times along the x and four along the y axis. Therefore, each layer parallel to the surface contains 64 Pt atoms. The replica of the unit cell along the z, i.e., perpendicular to the surface, is translated along the xy plane in order to maintain the fcc lattice of the Pt(111) crystal. Starting from the atomic positions of the bulk at equilibrium, i.e., with the GPW equilibrium lattice constant, the (111) surface structure has been optimized by means of the BFGS procedure, but keeping fixed the atoms of the two bottom-most layers. In this way,

we guarantee that, also for the thinner slabs, some of the layers maintain a bulklike structure. The slab supercell exposing the (100) surface has been generated by simply replicating the conventional unit cell $(4\times4\times4)$ times along the Cartesian axis. The resulting supercell is shown in Fig. 1(a). This supercell exposes a surface parallel to the xy plain containing 32 Pt atoms and is formed by eight atomic layers piled along the z axis. Also in this case, we used the bulk equilibrium positions as starting configuration. However, the surface relaxation has been obtained following two different procedures. In one case, the two bottom-most layers have been kept fixed during the BFGS optimization, as for the (111) slab. In the second case, the two central layers have been kept fixed, thus obtaining a symmetric slab with two fully relaxed (100) surfaces.

B. PW simulations

Calculations using the standard PW approach in combination with the k-point expansion have been carried out with two different program packages, ABINIT (Ref. 52) and PWSCF (Ref. 53). With ABINIT we used the same functional (PBE) and the same Goedecker–Teter–Hutter PP employed for GPW calculations. Structural and electronic properties of the bulk have been calculated using the unit cell of four Pt atoms, but varying from 20 to 120 Ry the energy cutoff for the expansion of the wave functions in PW, and testing several MP k-point meshes, from $(2\times2\times2)$ to $(10\times10\times10)$. The atomic positions and the volume have been optimized simultaneously by the application of a combined BFGS algorithm that exploits the calculation of the stress tensor to update the cell vectors at each iteration of the geometry optimizer. We found that with cutoff energy of 80 Ry and the $(6\times6\times6)$ k-point mesh the total energy is converged within 1 mHartree/atom and the equilibrium lattice constant within 1 mÅ. To estimate the bulk modulus, 13 geometry optimization runs have been performed at constant volume, varying the lattice constant between 3.90 and 4.02 Å with increments of 0.01 Å. For these latter simulations, a PW cutoff of 80 Ry and the $(10\times10\times10)$ k-point mesh have been used.

For PWSCF, ultrasoft PPs were used for Pt and PBE (Ref. 60) GGA was used for the exchange and correlation functional. No s, p semicore electrons were included. Wave functions were expanded in PW with a cutoff of 30 Ry, and the charge density was expanded in PW with a cutoff of 240 Ry. The Pt(111) surface was modeled using unit cells of 8 or 16 layers with 2 Pt atoms per layer. The initial coordinates were chosen according to the equilibrium lattice constant for the bulk (4.00 Å). An unshifted grid of $(8\times4\times1)$ was applied to compare the results to the GPW data. The Pt(100) surface was modeled by means of a unit cell containing eight layers with two Pt atoms per layer. The initial coordinates were chosen according to the equilibrium lattice constant for the bulk (4.00 Å). The integration of the BZ was performed with an unshifted grid of $(4\times4\times1)$ in order to directly compare the results with the GPW data.

C. Description of the geometrical and electronic properties

1. Structural properties of bulk Pt and Pt surfaces

We select two parameters to evaluate the description of the structural properties of the bulk with the different approaches, the equilibrium lattice constant a_0, and the bulk modulus B_0. The standard procedure to determine B_0 is through Murnaghan's equation,[67] which relates the variation in total energy to changes in volume via the bulk modulus and its first derivative. Therefore, these two parameters can be extracted from the least-squares fitting of the computed energy versus volume curve via the known analytical expression.

The characterization of the slab structures is done by measuring the variation in the interlayer distance with respect to the typical bulk value. The relative variation d_{rel} is estimated as a function of the depth of the layer inside the slab. Obviously, the more exposed is the layer, the larger is the structural rearrangement, whereas the innermost layers are expected to reproduce the bulk behavior, at least for the thickest samples. Possible surface reconstructions are not considered here. They would require the comparison between different putative structures and the evaluation of surface stress densities, which goes beyond the scope of this work. However, we must keep this limitation in mind when we consider the bulk-terminated Pt(100) face, since the stable structure of this surface has a close packed (111)-like reconstruction.

2. Density of states

By total density of states (TDOS) we indicate the distribution of the Kohn–Sham energies of occupied and unoccupied states,

$$n(E)=\sum_i \delta(\epsilon_i-E) \tag{2}$$

as computed without making any distinction either in terms of the character of the molecular orbital (s, p, or d) or with respect to spatial localization of the wave function. The projected, DOSs (PDOSs), instead, are obtained by selecting only the contributions with the desired orbital character. Within the GPW scheme, the PDOS is straightforwardly computed by projecting the molecular orbital onto a given subset of basis set functions. This is done with a procedure derived from the Löwdin population analysis, so that the d projected DOS can be written as

$$\begin{aligned} n_d(E) &= \sum_i \left[\sum_{\alpha\in d} |\langle \psi_i|\varphi_\alpha\rangle|^2 \delta(\epsilon_i-E) \right] \\ &= \sum_i \left[\sum_{\alpha\in d} (S^{1/2}P^iS^{1/2})_{\alpha\alpha} \right], \end{aligned} \tag{3}$$

where $S=[\langle\varphi_\alpha|\varphi_\beta\rangle]$ is the overlap matrix and $P^i=[C_{\gamma i}C_{\gamma' i}]$ is the density matrix associated with the ith state. Finally, localized DOS (LDOS) can also be easily defined by selecting in the expansion only those localized orbitals φ_α, which are centered on atoms located in the region of interest. All plots of the density of states presented in this work have been obtained as Gaussian convolutions of the computed discrete

distributions, using Gaussian functions with width of 0.2 eV. Moreover, the resulting curves have been normalized, with respect to the total number of states N, and shifted rigidly, in order to align the Fermi energy to the origin of the energy axis.

3. Center and filling of the d band

The center of the d band (ϵ_d) corresponds to the first moment of the density of states projected onto the d band.[68–70] It is therefore a measure of the integrated average energy from the lower to the upper edges of the d band, and it is computed as[71]

$$\epsilon_d = \frac{1}{N}\sum_i^N \epsilon_i \cdot w_i^d, \tag{4}$$

where w_i^d is the total contribution of the ith state to the d-PDOS and N is the total number of states. The filling of the d band (f_d) is a measure of the fraction of the occupied d orbitals and is determined as[68–70]

$$f_d = \frac{\sum_i^{\mathrm{occ}} w_i^d}{\sum_i^N w_i^d}. \tag{5}$$

4. Work function

The work function (Φ) of an infinitely extended solid surface with a given orientation is the minimum energy required to extract an electron from the Fermi level to a point at an infinite distance from the surface. The former definition is appropriate for slab calculations where a vacuum region is explicitly included in the model. Thus, the work function is most commonly evaluated by[72,73]

$$\Phi = \phi_0 - \epsilon_F, \tag{6}$$

where ϕ_0 is the electrostatic potential in the vacuum region, taken in the middle of the vacuum region, and ϵ_F is the Fermi level of the metal. A more accurate way to determine the work function exploits the separation of the Φ into a bulk contribution and a surface-dependent term,

$$\Phi = \Delta V - \epsilon_F^{\mathrm{bulk}}, \tag{7}$$

where $\epsilon_F^{\mathrm{bulk}}$ is the Fermi level for the bulk and ΔV is the potential difference between the metal and the vacuum. The potential within the metal is a macroscopic-average measure obtained by integration over the interplanar distance d of the slab,

$$\bar{\bar{V}}_{\mathrm{el}}(z) = \frac{1}{d}\int_{-d/2}^{d/2} \bar{V}_{\mathrm{el}}(z+z')dz',$$

where $\bar{V}_{\mathrm{el}}(z)$ is the plane-averaged potential

$$\bar{V}_{\mathrm{el}}(z) = S^{-1}\int_S V_{\mathrm{el}}(\mathbf{r})dxdy.$$

5. Surface energy

The surface energy (σ) is the energy per surface area needed to split an infinite crystal into two semi-infinite crystals.[24] Within the slab approximation, when symmetric slabs are used, exposing two equivalent surfaces, σ can be computed by

$$\sigma = \frac{1}{2A}(E_S^R - N_{\mathrm{at}}E_B), \tag{8}$$

where E_S^R is the total energy of a fully relaxed slab containing N_{at} atoms, $2A$ is the total surface area, and E_B is the reference bulk energy per atom. When asymmetric slabs are optimized by keeping fixed the bottom-most layers, the contribution of the unrelaxed surface has to be taken into account. The required correction can be easily determined by applying to a completely unrelaxed slab the same procedure described in Eq. (8),

$$\sigma_{\mathrm{UR}} = \frac{1}{2A}(E_S^{\mathrm{UR}} - N_{\mathrm{at}}E_B), \tag{9}$$

where E_{UR} is the total energy of the unrelaxed slab and σ_{UR} is the corresponding surface energy. The surface energy is then obtained as

$$\sigma = E_S - N_{\mathrm{at}}E_B - \sigma_{\mathrm{UR}}, \tag{10}$$

where E_S is the total energy computed for the asymmetric slab.

Since the accuracy of PW calculations performed with different simulations cell is not equivalent, using the bulk energy obtained from independent bulk calculations as reference energy for the slab calculations can introduce errors that linearly increase with the number of atoms. These problems have been known since long time.[29,74–76] The common work around is to define a consistent bulk energy per atom for each specific slab structure, by extrapolating it directly from the same slab calculation, i.e., keeping the volume of the simulation cell unchanged. This is done by progressively increasing the number of layers and taking the difference between the resulting total energies, divided by the number of additional "bulk" atoms. E_B then reads

$$E_B = (E_S^R(N+1) - E_S^R(N))/N_{\mathrm{atl}} = \frac{1}{N_{\mathrm{atl}}}\partial E_S^R(N)/\partial N, \tag{11}$$

where $E_S^R(N)$ is the total energy of the slab formed by N layers and N_{atl} is the number of atoms per layer, since only one layer has been added in this case. In the following discussion, we report surface energies obtained with both procedures.

III. RESULTS AND DISCUSSION

In the first part of this discussion, some structural and electronic properties of bulk Pt are considered and compared to the available experimental data. In the second part, the structural relaxation and the electronic properties of the closed-packed (111) surface and of the less stable and much less studied (100) surface are addressed. GPW calculations carried out on simulation cells of different sizes are compared to the results obtained with the PWSCF code and the ABINIT code. The goal is to demonstrate that localized basis sets and the supercell approach can be as accurate as standard PW methods in the description of a metallic system

TABLE I. Equilibrium lattice constant (a_0) and bulk modulus (B_0) for the bulk Pt calculated with the GPW formalism as a function of the size of the supercell. The results are compared with new PW calculations [PW(1) and PW(2)] at *k*-point convergence, theoretical PW simulations available in the literature [FP-LAPW(1) (Ref. 24), FP-LAPW(2) (Ref. 77), and CO-LCAO (Ref. 26)], and the experimental data (Refs. 78 and 104).

Simulation	a_0 (Å)	B_0 (GPa)
GPW $(3\times3\times3)$	3.955	272
GPW $(4\times4\times4)$	3.965	260
GPW $(5\times5\times5)$	3.965	265
GPW $(6\times6\times6)$	3.965	270
PW(1)	4.000	239
PW(2)	3.963	261
FP-LAPW(1)[a]	3.970	241
FP-LAPW(2)[b]	3.980	259
CO-LCAO[c]	3.990	270
Expt	3.92[d]	278[e]

[a]Reference 24.
[b]Reference 77.
[c]Reference 26.
[d]Reference 78.
[e]Reference 104.

such as Pt. In what follows, we label as PW(1) results obtained with PWSCF and PW(2) those obtained with ABINIT. If not differently specified, the reported values are those obtained at convergence with respect to energy cutoff and *k*-point mesh. We also mention results published in other DFT works on Pt.[24,26,77] Da Silva *et al.* studied the bulk and clean (111) surfaces for several transition metals by using all electron full-potential linearized augmented PWs (FP-LAPW) calculations.[24] We label with FP-LAPW(1) their FP-LAPW results as obtained for Pt bulk and Pt(111) with the PBE functional. Baud *et al.* reported a comparative study between the FP-LAPW method and the tight binding method of Pt(111) and Pt(100) surfaces.[77] FP-LAPW(2) indicates their results with the FP-LAPW method. Kokalj and Causa,[26] instead, to investigate bulk Pt and Pt(111), employed crystalline orbital LCAO (CO-LCAO) calculations. Their PBE results are here labeled with CO-LCAO.

A. Properties of bulk platinum

1. Structural properties

The equilibrium lattice constant (a_0) and the bulk modulus (B_0) for the bulk Pt calculated with the GPW approach as a function of the size of the supercell are shown in Table I. For each supercell, 13 independent geometry optimizations have been performed, varying the lattice constant from the experimental value of 3.920 up to 3.980 Å with a step of 0.005 Å. Table I reports also the available experimental values and some other theoretical results, as computed in the DFT works described above. The GPW equilibrium lattice constant was found at 3.965 Å for all the supercells except the smallest one, which gives a somewhat smaller value, 3.955 Å. The value is in excellent agreement with the ABINIT calculation, where exactly the same pseudopotentials have been used. In the calculation of B_0, the variability of the values is larger and there is no clear convergence trend by increasing the system size. However, the GPW results are in line with the other PW calculations, in particular, with PW(2), FP-LAPW(2), and CO-LCAO, and underestimate slightly the experimental value. The larger variations among the other PW calculations can be attributed to different models that have been employed. In particular, we observe that the ultrasoft PP used together with PWSCF gives the largest a_0 and the softest B_0. With respect to experiment,[78] we observe that our norm-conserving PP gives the best agreement in the equilibrium lattice constant, even slightly better than the all-electron value reported in FP-LAPW(1). We conclude that the bulk structural properties are well described by the GPW formalism, with the GTH PP and the TZV GTO basis set, already using a relatively small supercell containing 256 atoms $[(4\times4\times4)$ unit cells].

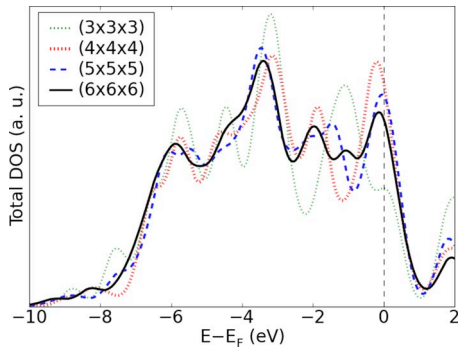

FIG. 2. (Color online) GPW-TDOS computed for bulk Pt as a function of the supercell size. The plots are Gaussian convolution of the discrete distribution. In order to facilitate the direct comparison, the Fermi energies have been aligned to zero eV and the curves have been normalized with respect to the number of states.

2. Electronic properties

Figure 2 shows the TDOS of bulk Pt, calculated with the GPW approach, as a function of the supercell size. The DOS obtained with the smallest box is the most structured, showing several distinguished peaks separated by pseudogaps. Moreover, at the Fermi energy the amounts of states are particularly low, forming a shoulder instead of the characteristic pronounced peak corresponding to the conduction band. This behavior can be attributed to the poor sampling of the BZ provided by such a small system. To compute the state distribution, we could rely, indeed, only on 1944 states, which is evidently not sufficient to reproduce accurately the electronic properties of the infinite bulk. With the $(4\times4\times4)$ box some smoothening is already visible, but the DOS profile is still too much structured above −3 eV, where a deep pseudogap is formed just before the conduction band crossed by the Fermi level. However, the presence of a pronounced peak around the Fermi energy reveals that the metallic character is reproduced. By further increasing the supercell, we obtained the expected rectangular shape of the DOS, where the Fermi level is located slightly above the center of the highest partially occupied conduction band. In particular, $(6\times6\times6)$ TDOS resembles closely the CO-LCAO results,[26] where the wave functions have been expanded over a total of 72

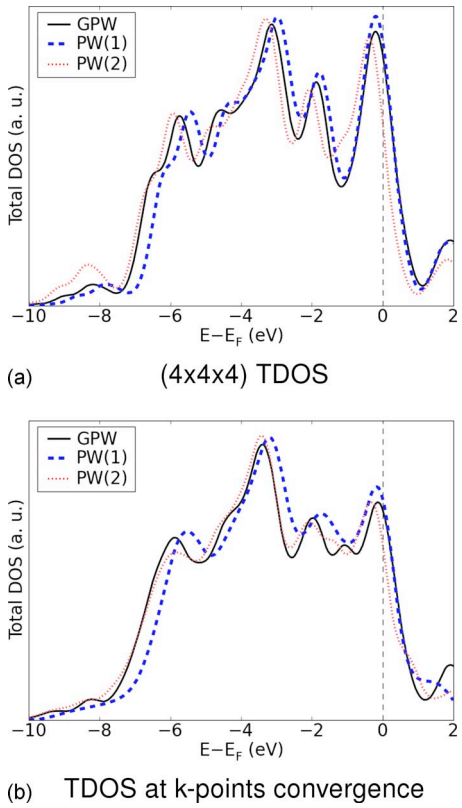

FIG. 3. (Color online) Comparison between the TDOS of bulk Pt as obtained with GPW and the two PW approaches (PWSCF and ABINIT) considered in this work. (a) GPW with the $(4\times4\times4)$ supercell compared to PW calculations performed with the $(4\times4\times4)$ MP grid. (b) GPW with the $(6\times6\times6)$ supercell compared to PW calculations that are converged with respect to the *k*-points mesh.

k-points of a MP grid, and it is also in good agreement with augmented PWs calculations reported in Ref. 79 using 128 *k*-points in the BZ.

The validation of the GPW electronic structure through the comparison of the DOS with respect to other published results can be done only qualitatively. A direct comparison in quantitative terms is instead possible by plotting the GPW-TDOS together with the curves extracted from the PW(1) and PW(2) simulations, thus using the same energy channel for the distribution and the same convolution scheme. We carried out two types of comparisons that are reported in Figs. 3(a) and 3(b). In the first case, the TDOSs obtained with the GPW and the PW approaches were compared at the same level of accuracy in terms of supercell size and *k*-point mesh, in order to assess the role of the different basis sets in the determination of the electronic properties. To this purpose, the $(4\times4\times4)$ GPW simulation has been compared to PWSCF and ABINIT calculations carried out on the unit cell by expanding the wave function over a $(4\times4\times4)$ MP grid. The similarity between the three distributions is striking. The curves show the same features and the only differences are small shifts of the peak centers and a slightly larger intensity of some of them, in particular, the one crossed by the Fermi energy. We conclude that, by selecting equivalent samplings of the BZ, the differences between the GPW and PW results in the description of the electronic states distribution lay within the uncertainty of the calculation.

Figure 3(b) shows the comparison between our best GPW calculation with the $(6\times6\times6)$ supercell and the PW(1) and PW(2) results obtained with the $(10\times10\times10)$ and the $(8\times8\times8)$ MP grids, respectively. In this manner, we want to demonstrate that selecting the proper simulation parameters, we can reach the same accuracy in the description of electronic structure of bulk Pt. The agreement between the three curves is again excellent. Same modifications are observed with respect to the less accurate sampling reported in the top panel of the same figure, irrespective of the specific formalism or PP.

The *s*, *p*, and *d* PDOSs computed from the GPW electronic structure of the $(6\times6\times6)$ supercell are reported in Fig. S1 in the Supplementary Material.[80] In the figure, the intensities of the the *s* and *p* PDOSs are very small in the displayed energy interval, therefore their plots have been magnified by a factor of 10. It is clear that within this energy range the TDOS is dominated by the *d* contributions, and only in the lowest energy part the *s* and *p* contributions are not negligible. The overall dimension of the *d* band is approximately 8.5 eV, while *s* and *p* states are distributed through the entire range of energies considered. All these properties are in excellent agreement with the theoretical data available in the literature, from CO-LCAO (Ref. 26) or from the calculations based on the APW approach.[79]

B. Properties of the Pt(111) surface

With the GPW approach the properties of the Pt(111) surface were evaluated as a function of the number of layers using large slabs exposing a surface of (8×8) Pt atoms. The number of layers of the slabs was increased from 3 to 8. Figure 1(b) shows the thickest supercell, with eight layers. The GPW simulations were compared to PWSCF calculations (PW(1)), by modeling the Pt(111) by a unit cell of eight layers with two Pt atoms per layer and expanding the wave function over a $(8\times4\times1)$ MP grid. This MP mesh has been selected to reproduce practically the same BZ sampling provided by the (8×8) supercell used with GPW. Table II summarizes some geometrical and electronic properties of Pt(111) as extracted from our GPW and PWSCF calculations. For the PW(1) calculations all atoms were allowed to relax. Our results are compared to the previously published values obtained by FP-LAPW [FP-LAPW(1) (Ref. 24) and FP-LAPW(2) (Ref. 77)] and CO-LCAO (CO-LCAO) (Ref. 26) calculations. The table reports also some available experimental data.[10,12,18,81,82]

1. Structural properties

Table II shows the interlayer relaxation distance between the first two layers of the slabs (d_{rel}). d_{rel} is an indicator of modifications of the surface layers when they relax from their bulk position. Since in the literature the d_{rel} is described either with the absolute value of the displacement (angstroms) or with the value relative to the interlayer distance in the bulk (%), in the present study both of the numbers are reported. Within the GPW calculations, although varying as a function of the number of layers, d_{rel} converge to a value in agreement with the experimental data.[10,12] The results are

TABLE II. Interlayer relaxation distance between the first two layers (d_{rel}), surface energies (σ), work function (Φ), center of the d band (ϵ_d), and filling of the d band (f_d) for the Pt(111) surfaces obtained from the GPW and PW calculations. The results are compared with the published theoretical [FP-LAPW(1) (Ref. 24), FP-LAPW(2) (Ref. 77), and CO-LCAO (Ref. 26)] and experimental data (Refs. 10, 12, 18, and 82). In the GPW and PW(1) calculations the number N of layers of the supercell is reported. σ^a is calculated with the bulk energy from a separate bulk calculation. σ^b is calculated by extrapolating the bulk energy from two slab calculations. Φ^a is calculated with Eq. (6). Φ^b is calculated with Eq. (7).

	N	d_{rel} (Å)	d_{rel} (%)	σ^a (eV)	σ^b (eV)	Φ^a (eV)	Φ^b (eV)	ϵ_d (eV)	f_d
GPW	3	0.015	0.67	0.77	0.73	5.79	5.68	−2.48	0.90
	4	0.005	0.22	0.74	0.69	5.69	5.77	−2.64	0.90
	5	0.013	0.59	0.75	0.68	5.70	5.70	−2.70	0.91
	6	0.029	1.26	0.73	0.64	5.64	5.56	−2.71	0.91
	7	0.015	0.63	0.70	0.60	5.60	5.66	−2.76	0.90
	8	0.026	1.12	0.71	0.60	5.61	5.66	−2.77	0.90
PW(1)	8	0.028	1.20	⋯	1.01	⋯	5.76	−2.66	0.90
FP-LAPW(1)[a]		⋯	1.14	⋯	0.70	5.69	⋯		
FP-LAPW(2)[b]		⋯	1.2	0.85	⋯	6.53[d]	⋯		
CO-LCAO[c]		0.017	⋯	⋯	0.70	⋯	⋯		
Expt		0.025 ± 0.01[e]	1.0 ± 0.1[f]		0.96[g]	5.7 ± 0.2[h]			

[a]Reference 24.
[b]Reference 77.
[c]Reference 26.
[d]LDA functional.
[e]Reference 10.
[f]Reference 12.
[g]Reference 82.
[h]Reference 18.

also in good agreement with the PW(1) calculations and with the theoretical simulations reported in the literature [FP-LAPW(1), FP-LAPW(2), and CO-LCAO].[24,26,77]

2. Electronic properties

For the GPW calculations the surface energy (σ) was evaluated as a function of the number of layers using Eq. (10). The bulk energy per atom E_B is either taken as the equilibrium energy of independent bulk calculations or it is extrapolated from two slab calculations by incrementing the number of layers, as described in Eq. (11). In Table II, results obtained by the former procedure are referred to as σ^a. In this case, E_B is the energy resulting from the geometry optimization of the $(6\times6\times6)$ supercell. σ^b, instead, are the surface energies obtained by the incremental approach, where E_B is obtained from the difference between the energies computed for the relaxed slabs formed by eight and seven layers.

As can be seen from Table II, by increasing the number of layers the surface energy converges to stable values. The converged value obtained with σ^a is in agreement with the published theoretical calculations,[24,26,77] while σ^b slightly underestimates the theoretical values. Although the bulk energy calculated with the two different methods only differs by 0.03 eV (data not shown), the effect on σ is clearly visible. The evaluation of the surface energy is therefore particularly affected by the correct determination of the total energy per atom of the bulk. It is striking that the σ^b evaluated using the PW formalism and a unit cell with eight layers [PW(1)] strongly overestimates the theoretical values. An identical PW calculation where the thickness of the slab is increased to 24 layers predicts a σ^b of 0.62 eV, in agreement with σ^b obtained with the GPW formalism. The surface energy is slightly faster converging with the GPW than with the PW formalism. This apparent advantage of GPW upon PW is likely to be accidental. The comparison with PW(1) shows that the GPW calculations are as accurate as PW simulations in the determination of the total energies of bulk Pt and Pt surfaces. Furthermore, with the GPW approach the convergence of the total energy is reached with thinner cells.

In Table II also the experimental surface energy is reported.[82] However, although the latter datum is reliable since it comes from an experiment done in the solid state, as pointed out in Ref. 83, Pt crystals at the experimental conditions (i.e., not far from the melting point) only expose high-symmetry faces for about 15% of their surface, the rest being stepped or faceted surfaces. Therefore, the comparison between the theoretical and experimental surface energies should be carefully considered.[24] While the consistency with the experiments is difficult to discuss, the agreement of the GPW simulations with the theoretical calculations based on classical PW, both new and published, is excellent.

The work function (Φ) of the Pt(111) surface was determined using Eqs. (6) and (7) reported in Sec. II. For the GPW simulations, Φ was calculated as a function of the number of layers. Using Eq. (6) Φ decreases continuously as the number of layers increases, while with Eq. (7) it converges to the value of 5.66 eV. The results are in good agreement with the theoretical calculations evaluated either by Eq. (6) [FP-LAPW(1)] or by Eq. (7) [PW(1)] and with the experimental value (5.7 eV).[18] The values from FP-LAPW(2) calculations are slightly overestimated. The larger prediction is due to the choice of a functional based on the LDA, which is known to overestimate the work function compared to GGA-based functionals. Feibelman proposed that the addition of the so-called floating orbitals may improve significantly the estimate of the work function if a local basis set was used.[84] In order to determine the effect of such floating orbitals in the prediction of the work function by the GPW

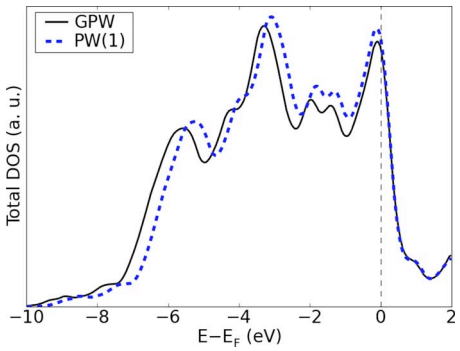

FIG. 4. (Color online) Comparison of the TDOS for the Pt(111) surface calculated with the GPW (eight layers) or the PW formalisms (eight layers 8×8 MP grid).

formalism, a simulation using the $(8\times8\times7)$ slab was performed, in which additional s and p floating orbitals were included on top of the relaxed surface, as described in detail in Ref. 84. A total of 128 s orbitals and 192 p orbitals were added. As an effect of the additional orbitals, the work function decreases by 0.01 eV, from 5.60 to 5.59 eV. Therefore, in this case, the work function seems to be almost unaffected by the presence of such floating orbitals.

In Table II the values of the center of the d band (ϵ_d) and the filling of the d band (f_d) are also included.[68–70] For the GPW simulations, the values were determined as a function of the number of layers from the plots reported in Fig. S2 in the Supplementary Material. For the Pt(111) surface ϵ_d was already published by different groups[3,85–88] and the results vary from −2.52 to −2.80 eV. The estimations obtained with the GPW and the PW formalisms are in accordance with the theoretical data reported by the above cited groups. The GPW-TDOSs of Pt(111) as a function of the number of layers in the slab are reported in Figure S2 in the Supplementary Material. Convergence is reached with slabs of five layers. Some minor differences are visible in the range from −2 to −1 eV.

The accuracy of the electronic description of the Pt(111) surface by means of the GPW formalism is confirmed by the direct comparison of the $(8\times8\times8)$ GPW-TDOS with the PW(1)-TDOS. The results are shown in Fig. 4. The LDOSs computed on the first layer of the Pt(111) slab are, instead, reported in Fig. S3 in the Supplementary Material. In both cases, the agreement between the curves obtained by the two approaches is striking.

All the structures observed in the PW(1)-TDOS are present in the GPW spectrum and the relative intensities of the peaks are also well reproduced. Around the Fermi level the two curves practically overlap, whereas at lower energy a slight translation of about +0.2–0.3 eV is observed. While the TDOSs are typically dominated by bulk contributions, the LDOSs in Figure S3 emphasize the effects of the surface on the state distribution. Once more, with both the approaches we observe the same behavior. In particular, the peak at −6 eV and the shoulder at approximately −4 eV largely decrease while the peaks at −1.8 and −2 eV undergo a significative increase.

The discussed agreement in the TDOS and the LDOS confirms the equivalence of the two formalisms also in the description of the surface electronic properties of Pt(111). We conclude that, when equivalent supercell and k-point mesh are employed, the GPW method guarantees the same accuracy as standard PW schemes, for structural as well as electronic properties of Pt surfaces.

C. Properties of the Pt(100) surface

In order to give a broader and more complete survey of the comparison between GPW and PW formalisms, the analysis of the Pt surface is extended to the less studied and more reactive (100) surface. Since the larger slab calculated for the Pt(111) surface had eight layers, the Pt(100) surface was modeled using a supercell with eight layers.

For the simulations with the GPW, the Pt(100) surface has been modeled by the supercell shown in Fig. 1(a), using the equilibrium lattice constant obtained for the bulk Pt (3.965 Å). As specified in Sec. II, two different protocols have been applied to mimic the bulk behavior of the internal layers of the slab. Either the two bottom-most layers were fixed, by constraining the atomic coordinates to the corresponding bulk positions [GPW(1)], or the two central layers were fixed [GPW(2)], thus giving a symmetric slab. The PW calculations were run with the PWSCF software [PW(1)]. In the latter case the Pt(100) surface was modeled by a supercell of eight Pt layers with two Pt atoms per layer. An unshifted $(4\times4\times1)$ k-point sampling was used to guarantee equivalence with the Γ-point calculations.

1. Structural properties

Table III shows the relaxation distance (d_{rel}) between the first two layers. Numerous experimental investigations on the Pt(100) surface structure have been reported in the literature, based on LEEDS, Rutherford backscattering (RBS), helium diffraction, or scanning tunneling microscopy.[89–100]

TABLE III. Interlayer relaxation distance between the first two layers (d_{rel}), work function (Φ), center of the d band (ϵ_d), and filling of the d band (f_d) for the Pt(100) surfaces calculated with the GPW and PW formalisms. GPW(1) refers to a GPW calculation in which the two bottom-most layers were fixed, while GPW(2) refers to a GPW calculation in which the two central layers were fixed, thus giving a symmetric slab. Φ^a is calculated with Eq. (6). Φ^b is calculated with Eq. (7).

	d_{rel} (Å)	d_{rel} (%)	Φ^a (eV)	Φ^b (eV)	ϵ_d (eV)	f_d
GPW(1)	−0.028	−1.42	5.32	5.22	−2.88	0.93
GPW(2)	−0.028	−1.40	5.32	5.17	−2.88	0.93
PW(1)	−0.042	−2.18	⋯	5.64	−2.62	0.91

Since it is known that the Pt(100) easily reconstructs, most of these studies focus the reconstruction process itself. Although experimental LEED and RBS evidences have been used to develop models of the reconstruction of the surface, they were not completely satisfactory about the relaxation displacements in the direction normal to the surface. Using LEED, Somorjai and co-workers reported a contraction of the first layer in the range from −4.2% to 12.6% with respect to the bulk.[94,95] Other results based on LEED published by Titmuss *et al.* showed an expansion of the first layer by 0.0 ± 5.1 and 0.2 ± 2.6 Å.[98] RBS experiments reveal only a small thickening of the slab by 0.01 ± 0.01 Å. Since the experimental results were not conclusive, the GPW and PW simulations were only compared theoretically. While for the Pt(111) surface the topmost layers expanded with respect to the positions of the bulk, for the Pt(100) the surface layers slightly shrank compared to the bulk. The GPW(1) and GPW(2) simulations produce the same geometric displacement of the topmost layers. Compared to the displacements observed for the PW(1) calculation, the d_{rel} predicted by the GPW(1) and GPW(2) simulations are slightly lower. The theoretical displacements are in the order of magnitude of only a few percents of the interlayer distance. Interestingly, the GPW and PW formalisms predict a contraction of the less compact Pt(100) surface relatively to the Pt(111) surface. This seems to agree with general conclusion found in the relevant literature.[8]

2. Electronic properties

With the GPW formalism the work function Φ was determined using both Eqs. (6) and (7), while for the PW(1) calculation Φ was determined with Eq. (6). For the GPW calculations the results obtained using Eq. (6) are to a small degree higher than the results obtained with Eq. (7). The GPW(1) and GPW(2) calculations are to a certain extent underestimating the experimental value (5.65 eV) (Ref. 101) and the theoretical value reported by the PW(1) simulation (5.64 eV). Compared to the work function of the Pt(111) surface (Table II), the Φ for the Pt(100) was lower for both the GPW and the PW(1) calculations. This result is explained in terms of the Smoluchowski effect: at the surface, in the absence of the next ionic layer, the electrons are less bound to the metal.[102,103] Their charge density can therefore spread into the vacuum, creating a surface dipole which generates an electric field, responsible for the work function. However, the charge density is corrugated along the surface plane, and the electrons try to reduce this corrugation, basically for reducing their kinetic energy which is connected to the spatial gradient of the wave function. This smoothing phenomenon reduced the previously cited surface dipole, and thus the work function. However, this smoothing effect is less pronounced for close packed surfaces, so that the reduction in the work function is more evident for the less close packed (100) face of a metal. Consequently, the Pt(111) surface should have a higher Φ than the Pt(100) surface. Although the difference is more pronounced in the case of the PW simulations than in the case of the GPW calculations, the scale of stability of the Pt surface is correctly predicted by the theoretical simulations performed in the study.

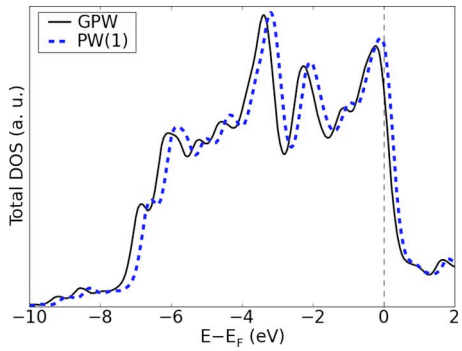

FIG. 5. (Color online) Comparison of the TDOS relative to the Fermi level for the Pt(100) surface calculated with the GPW and PW formalisms. PW(1) refers to the simulations with PWSCF software package.

The center of the *d* band with respect to the Fermi energy (ϵ_d) and the filling of the *d* band (f_d) are also reported in Table III. These properties are calculated from the plots in Fig. 5. Once again, the GPW(1) and GPW(2) simulations are undistinguishable. The high agreement between the GPW(1) and GPW(2) results indicates that the relaxation protocol has a negligible influence in the determination of both the geometrical and electronic properties of the Pt surface. The f_d evaluated with the GPW(1), GPW(2), and PW(1) calculations are in agreement. The difference of approximately 0.3 eV between the ϵ_d calculated with the GPW and the PW formalisms reflects the differences in the TDOS.

Figure 5 shows the TDOS of the Pt(100) surface calculated with the GPW method [GPW(1)] and the PW method with the PWSCF software [PW(1)]. The curves are in good agreement, and the main difference consists only in a shift by 0.3 eV of the PW(1) curve toward higher energies. This shift accounts for the 0.3 eV difference between the ϵ_d calculated with the GPW and PW formalisms. The correspondence between the TDOS obtained with the two approaches is a further indication of the reliability of GPW in the description of Pt surfaces. Once more, when equivalent supercell and MP mesh are employed, we observe the expected consistency of the results. Moreover, the validity of the different relaxation procedures is also confirmed by the obtained agreement in structural and electronic properties of the surface. Hence, the different protocols can all be used, providing that the slab is thick enough.

IV. CONCLUSIONS

In this study, the properties of bulk Pt and Pt surfaces have been investigated using the GPW formalism in comparison to the well established PW approach, in order to assess the accuracy of GPW simulations in the determination of the properties of Pt solids.

For the bulk Pt the theoretical equilibrium lattice constant, the bulk modulus, and the TDOS were studied as a function of the size of the supercell. In the case of the GPW simulations, the transition metal bulk was modeled using large supercells obtained by replicating a small unit cell of four Pt atoms ($n \times n \times n$) times, with *n* increased from 3 to 6. For the PW calculations, the bulk Pt was simulated with a small unit cell of four Pt atoms and different sampling of the

k-points. Two different sets of PW calculations were performed differing for the PP and the software used. For the GPW simulations, the equilibrium lattice constant is 3.965 Å and the bulk modulus is in the range of 260–270 GPa, in agreement with the experimental data and other theoretical calculations. Increasing the size of the supercell the TDOS of bulk Pt calculated with the GPW approach converged to a defined shape. Furthermore, the agreement of the TDOS obtained with the GPW and the PW formalisms is excellent. The data show that the structural and electronic properties of the bulk Pt are well described by the GPW formalism.

For the Pt(111) surface, the convergence of the structural and electronic properties of slabs with (8×8) Pt atoms per layer was studied with the GPW formalism as a function of the number of layers. It is shown that using slabs with eight layers the structural properties, the surface energy, the work function, and the center of the *d* band are converged and in good agreement with both the published theoretical data and the experiments. In particular, the TDOS is already converged using a supercell with five layers. The GPW simulations were compared with new PW simulations where the Pt(111) slabs were modeled by a unit cell of eight layers with two Pt atoms per layer and an unshifted grid of $(8\times4\times1)$. The structural and electronic properties are predicted with the same accuracy with the GPW and the PW formalism. In particular, the TDOS evaluated with the GPW formalism shows an excellent agreement with the TDOS calculated with the PW approach.

In the last part of the study, the results obtained with the GPW and the PW formalisms for the Pt(100) surface were compared. The Pt(100) surface was modeled for the GPW simulations with a supercell consisting of 256 Pt atoms, while the correspondent Pt(100) surface for the PW simulations was modeled with a unit cell of 4 Pt atoms and with an unshifted $(4\times4\times4)$ *k*-points sampling. The structural and electronic properties of the Pt(100) surface as determined by the GPW and PW formalisms converge to the same results. The convergence of the TDOS calculated with the two approaches is excellent.

The convergence of the results from GPW and PW calculation and of the electronic properties, in particular, show that the GPW method is a valuable and accurate tool for the description of the Pt bulk and surface, and it can be exploited in the theoretical investigation of large and complex systems of chemical interest.

ACKNOWLEDGMENTS

Financial support from the Swiss National Science Foundation is kindly acknowledged. The Swiss National Supercomputing Centre (CSCS, Manno) and ETHZ are acknowledged for providing computing resources.

[1] A. Gross, *Theoretical Surface; A Microscopic Perspective* (Springer-Verlag, Berlin, 2003).
[2] J. Greeley, J. K. Nørskov, and M. Mavrikakis, Annu. Rev. Phys. Chem. **53**, 319 (2002).
[3] B. Hammer and J. K. Nørskov, Adv. Catal. **45**, 71 (2000).
[4] M. Scheffler and C. Stampfl, *HandBook of Surface Science* (Elsevier, Amsterdam, 1999), Vol. 2.
[5] R. A. van Santen and M. Neurock, *Handbook of Heterogeneous Catalysis* (Wiley-VCH, Weinheim, 1997), Vol. 3.
[6] V. P. Zhdanov and B. Kasemo, Surf. Sci. Rep. **29**, 31 (1997).
[7] M. C. Desjonqueres and D. Spanjard, *Concepts in Surface Science* (Springer-Verlag, Berlin, 1995).
[8] G. A. Somorjai, *Introduction to Surface Chemistry and Catalysis* (Wiley Intersciences, New York, 1994).
[9] R. Gomer, Acc. Chem. Res. **29**, 284 (1996).
[10] N. Materer, U. Starke, A. Barbieri, R. Doll, K. Heinz, M. A. Van Hove, and G. A. Somorjai, Surf. Sci. **325**, 207 (1995).
[11] N. Materer, A. Barbieri, D. Gardin, U. Starke, J. D. Batteas, M. A. Van Hove, and G. A. Somorjai, Surf. Sci. **303**, 319 (1994).
[12] D. L. Adams, H. B. Nielsen, and M. A. Van Hove, Phys. Rev. B **20**, 4789 (1979).
[13] L. L. Kesmodel, P. C. Stair, and G. A. Somorjai, Surf. Sci. **64**, 342 (1977).
[14] J. A. Davies, D. P. Jackson, P. R. Norton, D. E. Posner, and W. N. Unertl, Solid State Commun. **34**, 41 (1980).
[15] J. F. van der Veen, R. G. Smeenk, R. M. Tromp, and F. W. Saris, Surf. Sci. **79**, 219 (1979).
[16] E. Bogh and I. Stensgaard, Phys. Lett. **65A**, 357 (1978).
[17] V. M. Tapilin, D. Y. Zemlyanov, M. Y. Smirnov, and V. V. Gorodetskii, Surf. Sci. **310**, 155 (1994).
[18] G. B. Fisher, Chem. Phys. Lett. **79**, 452 (1981).
[19] N. D. Lang and W. Kohn, Phys. Rev. B **7**, 3541 (1973).
[20] N. D. Lang and W. Kohn, Phys. Rev. B **3**, 1215 (1971).
[21] N. D. Lang and W. Kohn, Phys. Rev. B **1**, 4555 (1970).
[22] N. D. Lang, Solid State Commun. **9**, 1015 (1971).
[23] N. D. Lang, Phys. Rev. B **4**, 4234 (1971).
[24] J. L. F. Da Silva, C. Stampfl, and M. Scheffler, Surf. Sci. **600**, 703 (2006).
[25] W. K. Offermans, A. P. J. Jansen, and R. A. van Santen, Surf. Sci. **600**, 1714 (2006).
[26] A. Kokalj and M. Causa, J. Phys.: Condens. Matter **11**, 7463 (1999).
[27] L. Reinaudi, M. Del Popolo, and E. Leiva, Surf. Sci. **372**, L309 (1997).
[28] J. C. Boettger, Phys. Rev. B **53**, 13133 (1996).
[29] J. C. Boettger and S. B. Trickey, Phys. Rev. B **45**, 1363 (1992).
[30] M. Causa and A. Zupan, Int. J. Quantum Chem. **52**, 633 (1994).
[31] M. Causa and A. Zupan, Chem. Phys. Lett. **220**, 145 (1994).
[32] H. L. Skriver and N. M. Rosengaard, Phys. Rev. B **46**, 7157 (1992).
[33] I. P. Batra, S. Ciraci, G. P. Srivastava, J. S. Nelson, and C. Y. Fong, Phys. Rev. B **34**, 8246 (1986).
[34] P. J. Feibelman and D. R. Hamann, Phys. Rev. B **29**, 6463 (1984).
[35] P. Hohenberg and W. Kohn, Phys. Rev. **136**, B864 (1964).
[36] W. Kohn and L. J. Sham, Phys. Rev. **140**, 1133 (1965).
[37] P. C. Rusu and G. Brocks, Phys. Rev. B **74**, 073414 (2006).
[38] R. Dronskowski, *Computational Chemistry of Solid State Materials* (Wiley-VCH, Weinheim, 2005).
[39] H. J. Monkhorst and J. D. Pack, Phys. Rev. B **13**, 5188 (1976).
[40] G. Santarossa, M. Iannuzzi, A. Vargas, and A. Baiker, ChemPhysChem **9**, 401 (2008).
[41] A. Vargas, G. Santarossa, M. Iannuzzi, and A. Baiker, J. Phys. Chem. C **112**, 10200 (2008).
[42] K. Lee, J. Yu, and Y. Morikawa, Phys. Rev. B **75**, 045402 (2007).
[43] C.-C. Fu and F. Willaime, Phys. Rev. Lett. **92**, 175503 (2004).
[44] V. M. García-Suárez, C. M. Newman, C. J. Lambert, J. M. Pruneda, and J. Ferrer, J. Phys.: Condens. Matter **16**, 5453 (2004).
[45] J. M. Soler, E. Artacho, J. D. Gale, A. García, J. Junquera, P. Ordejón, and D. Sánchez-Portal, J. Phys.: Condens. Matter **14**, 2745 (2002).
[46] J. Izquierdo, A. Vega, L. C. Balbás, J. Junquera, E. Artacho, J. M. Soler, and P. Ordejón, Phys. Rev. B **61**, 13639 (2000).
[47] J. S. Nelson, A. F. Wright, S. J. Plimpton, P. A. Schultz, and M. P. Sears, Phys. Rev. B **52**, 9354 (1995).
[48] URL http://www.crystal.unito.it/.
[49] URL http://www.uam.es/departamentos/ciencias/fismateriac/siesta/.
[50] G. Lippert, J. Hutter, and M. Parrinello, Mol. Phys. **92**, 477 (1997).
[51] G. Lippert, J. Hutter, and M. Parrinello, Theor. Chem. Acc. **103**, 124 (1999).
[52] X. Gonze, J. Beuken, R. Caracas, F. Detraux, M. Fuchs, G. Rignanese, L. Sindic, M. Verstraete, G. Zerah, F. Jollet, M. Torrent, A. Roy, M. Mikami, P. Ghosez, J. Raty, and D. Allan, Comput. Mater. Sci. **25**, 478 (2002).
[53] S. Baroni, www.pwscf.org.
[54] S. Goedecker, Rev. Mod. Phys. **71**, 1085 (1999).
[55] J. VandeVondele, M. Krack, F. Mohamed, M. Parrinello, T. Chassaing,

and J. Hutter, Comput. Phys. Commun. **167**, 103 (2005).
[56] M. Krack and M. Parrinello, Phys. Chem. Chem. Phys. **2**, 2105 (2000).
[57] G. Hura, D. Russo, R. Glaeser, T. Head-Gordon, M. Krack, and M. Parrinello, Phys. Chem. Chem. Phys. **5**, 1981 (2003).
[58] I. Kuo, C. Mundy, M. McGrath, J. Siepmann, J. VandeVondele, M. Sprik, J. Hutter, B. Chen, M. Klein, F. Mohamed, M. Krack, and M. Parrinello, J. Phys. Chem. B **108**, 12990 (2004).
[59] S. Goedecker, M. Teter, and J. Hutter, Phys. Rev. B **54**, 1703 (1996).
[60] J. P. Perdew, K. Burke, and M. Ernzerhof, Phys. Rev. Lett. **77**, 3865 (1996).
[61] J. VandeVondele and J. Hutter, J. Chem. Phys. **118**, 4365 (2003).
[62] C. Broyden, Math. Comput. **24**, 365 (1970).
[63] J. Nocedal, Math. Comput. **35**, 773 (1980).
[64] D. Liu and J. Nocedal, SIAM (Soc. Ind. Appl. Math.) J. Sci. Stat. Comput. **10**, 1 (1989).
[65] D. Shanno and P. Kettler, Math. Comput. **24**, 657 (1970).
[66] D. Goldfarb, Math. Comput. **24**, 23 (1970).
[67] F. D. Murnaghan, Proc. Natl. Acad. Sci. U.S.A. **30**, 244 (1944).
[68] B. Hammer, Y. Morikawa, and J. K. Nørskov, Phys. Rev. Lett. **76**, 2141 (1996).
[69] B. Hammer and J. K. Nørskov, Surf. Sci. **343**, 211 (1995).
[70] B. Hammer and J. K. Nørskov, Nature (London) **376**, 238 (1995).
[71] J. Kitchin, J. K. Nørskov, M. Barteau, and J. Chen, J. Chem. Phys. **120**, 10240 (2004).
[72] F. K. Schulte, Surf. Sci. **55**, 427 (1976).
[73] F. K. Schulte, J. Phys. C **7**, L370 (1974).
[74] V. Fiorentini and M. Methfessel, J. Phys.: Condens. Matter **8**, 6525 (1996).
[75] J. C. Boettger, J. R. Smith, U. Birkenheuer, N. Rosch, S. B. Trickey, J. R. Sabin, and S. P. Apell, J. Phys.: Condens. Matter **10**, 893 (1998).
[76] J. C. Boettger, Phys. Rev. B **49**, 16798 (1994).
[77] S. Baud, C. Ramseyer, G. Bihlmayer, S. Blugel, C. Barreteau, M. C. Desjonqueres, D. Spanjaard, and N. Bernstein, Phys. Rev. B **70**, 235423 (2004).
[78] P. Villars and L. Calvert, *Pearson's Handbook of Crystallographic Data for Intermetallic Phases*, 2nd ed. (ASM International, Materials Park, OH, 1991).
[79] A. H. MacDonald, J. M. Daams, S. H. Vosko, and D. D. Koelling, Phys. Rev. B **23**, 6377 (1981).
[80] See EPAPS Document No. E-JCPSA6-129-802847 for the PDOS of bulk Pt and the convergence of the TDOS of the Pt(111) surface calculated with the GPW formalism, the comparison of the LDOS of the first layer of the Pt(111) surface calculated with the GPW and PW formalisms, and the complete relaxation details of the Pt(111) and the Pt(100) surfaces. For more information on EPAPS, see http://www.aip.org/pubservs/epaps
[81] W. R. Tyson and W. A. Miller, Surf. Sci. **62**, 267 (1977).
[82] V. Kuminkov and K. Khokonov, J. Appl. Phys. **54**, 1346 (1983).
[83] W. Lee, K. Vanloon, V. Petrova, J. Woodhouse, C. Loxton, and R. Masel, J. Catal. **126**, 658 (1990).
[84] P. J. Feibelman, Phys. Rev. B **51**, 17867 (1995).
[85] Y. Xu, A. Ruban, and M. Mavrikakis, J. Am. Chem. Soc. **126**, 4717 (2004).
[86] M. Mavrikakis, B. Hammer, and J. K. Nørskov, Phys. Rev. Lett. **81**, 2819 (1998).
[87] L. Wang and D. Johnson, J. Phys. Chem. C **112**, 8266 (2008).
[88] V. R. Stamenkovic, B. Fowler, B. S. Mun, G. Wang, P. N. Ross, C. A. Lucas, and N. M. Markovic, Science **315**, 493 (2007).
[89] R. J. Behm, W. Hösler, E. Ritter, and G. Binning, Phys. Rev. Lett. **56**, 228 (1986).
[90] H. P. Bonzel, C. R. Helms, and S. Kelemen, Phys. Rev. Lett. **35**, 1237 (1975).
[91] A. Borg, A. Hilmen, and E. Bergene, Surf. Sci. **306**, 10 (1994).
[92] J. A. Davies, T. Jackman, D. P. Jackson, and P. R. Norton, Surf. Sci. **109**, 20 (1981).
[93] X. Guo, A. Hopkinson, J. Bradley, and D. A. King, Surf. Sci. **278**, 263 (1992).
[94] S. Hagstrom, H. Lyon, and G. A. Somorjai, Phys. Rev. Lett. **15**, 491 (1965).
[95] M. V. Hove, R. Koestner, P. C. Stair, J. Biberian, L. L. Kesmodel, I. Bartos, and G. A. Somorjai, Surf. Sci. **103**, 189 (1981).
[96] P. Heilmann, K. Heinz, and K. Müller, Surf. Sci. **83**, 487 (1979).
[97] P. R. Norton, J. A. Davies, D. P. Jackson, and N. Matsunami, Surf. Sci. **85**, 269 (1979).
[98] S. Titmuss, A. Wander, and D. A. King, Chem. Rev. (Washington, D.C.) **96**, 1291 (1996).
[99] P. Watson, M. V. Hove, and K. Hermann, J. Phys. Chem. Ref. Data **1B**, 1 (1994).
[100] P. Watson, M. V. Hove, and K. Hermann, J. Phys. Chem. Ref. Data **1A**, 1 (1994).
[101] K. Wandelt, *Thin Metal Films and Gas Chemisorption* (Elsevier, Amsterdam, 1984).
[102] C. J. Fall, N. Binggeli, and A. Baldereschi, Phys. Rev. B **61**, 8489 (2000).
[103] R. Smoluchowski, Phys. Rev. **60**, 661 (1941).
[104] C. Kittel, *Introduction to Solid State Theory* (Wiley, New York, 1986).